Probing the Early Stages of Melt Crystallization in Polypropylene by Simultaneous Small- and Wide-Angle X-ray Scattering and Laser Light Scattering

Zhi-Gang Wang and Benjamin S. Hsiao*

Department of Chemistry, State University of New York at Stony Brook, Stony Brook, New York 11794-3400

Eric B. Sirota*

Exxon Mobil Research and Engineering Co., Corporate Strategic Research, Annandale, New Jersey 08801

Pawan Agarwal and Srivatsan Srinivas

Exxon Chemical Company, Baytown Polymers Center, Texas 77522-5200

Received August 27, 1999; Revised Manuscript Received December 7, 1999

ABSTRACT: The early stages of polymer melt crystallization using fractionated isotactic polypropylene (*i*PP) as a model system were investigated via simultaneous synchrotron small-angle X-ray scattering (SAXS)/wide-angle X-ray diffraction (WAXD) and laser light scattering (LS) techniques. Since the crystallinity in the early stages is very low, the issue of the crystallinity detection limit of WAXD was addressed. This was done by using solutions of *n*-paraffin ($C_{33}H_{68}$) in dodecane ($C_{12}H_{26}$) at different concentrations (as low as 1%). The precipitated fraction simulated the degree of crystallinity in polyethylene since *n*-paraffin essentially completely crystallized and dodecane remained liquid at the measurement temperature. A modeling method was also used to simulate the WAXD profiles to check the effect of crystal size at low crystallinity. With these two methods, we conclude that our WAXD procedure is capable of detecting crystallinity from 0.5% to 1%. During the early stages of *i*PP isothermal crystallization, noticeable short-range density fluctuations with average periods from 20 to 24 nm (by SAXS) were seen prior to the observation of three-dimensional ordering of the crystalline α-form (by WAXD). The spacing associated with the peak of the SAXS was found not to increase with time, being constant or a possible initial decrease, which is consistent with the formation of a finite lamellar structure. Furthermore, larger objects with dimensions growing from 300 nm were observed with the more sensitive technique of polarized light scattering, prior to the detection of the lamellar period by SAXS. The development of the crystallinity as measured by WAXD as well as SAXS and light scattering are all consistent, which follow the same Avrami equation, suggesting that the early stages of crystallization as measured here follow classical nucleation and growth.

Introduction

The behavior of the early stages of polymer crystallization from solution, glassy state, and molten state has been recently under intensive investigation. The difficulty in probing this regime are the weak signals from the small volume fraction involved in the early stages of crystallization, combined with the detection limits of the various techniques. The most common and simplest explanation for the early stages of crystallization is classical nucleation and growth. Before declaring a need for an alternative mechanism, we need to determine whether the experimental data exhibit any deviation from what would be expected from conventional nucleation and growth.

It has been argued that in dilute solutions polymer chains should collapse into a globular state prior to the formation of folded-chain single crystals upon crystallization.[1] Little experimental results exist in this area, but the argument is supported by recent molecular simulation work of Liu and Muthukumar.[2] During cold crystallization from the quenched glassy state in polymers such as poly(ethylene terephthalate), PET, and poly(aryl ether ketone ketone), PEKK, it was reported that the small-angle X-ray scattering (SAXS) peak appeared before the wide-angle X-ray diffraction (WAXD) crystalline peaks.[3−8] It was thought that the SAXS peak resulted from density fluctuations on the order of 5−30 nm, while WAXD crystalline peaks were brought about by three-dimensional crystal ordering on the order of 0.2−1 nm. The appearance of the SAXS peak before the WAXD crystalline peaks led to suggestions that density fluctuations occurred prior to crystallization in these samples. The initial behavior of the SAXS peak was argued to be consistent with the Cahn−Hilliard theory for spinodal decomposition;[9,10] i.e., the SAXS peak intensity grew exponentially with time whereas the peak position remained constant.

Some recent studies of isotactic polypropylene, *i*PP,[11,12] indicate that this behavior may also hold true during melt crystallization. Several authors have even suggested that density fluctuations, consistent with spinodal decomposition, may act as a precursor to crystallization.[4−8,11,12] Recently, Olmsted et al.[13] have proposed a theory arguing that the coupling of density and chain conformation can induce a liquid−liquid phase separation within the liquid−solid (crystal) boundary curve if the polymer melt is quenched below the spinodal curve. The two hypothesized coexistent liquids differ from each other in their distribution of chain conformations, which

* To whom correspondence should be addressed. E-mail: bhsiao@notes.cc.sunysb.edu; ebsirot@erenj.com.

10.1021/ma991468t CCC: $19.00
Published on Web 01/18/2000

was proposed to be the cause of the SAXS peak in the early stages. The specific structural difference of these two liquids, however, has not been identified. The hypothesis for the presence of spinodal decomposition like density fluctuations in the quenched glass can be rationalized in that the quenched liquid may retain a large degree of "frozen" nonequilibrium structures due to its long relaxation times. But the suggestion of the spinodal decomposition behavior in the precrystallizing melt has provoked significant challenges to the conventional theories of crystallization from the polymer melt. Regardless of what the correct mechanism may be, it is clear that new mechanisms have been proposed where the early stages of crystallization may deviate from the classic theories of nucleation and growth.

A well-documented case of deviation from the simple process of nucleation and growth at the early stages of melt crystallization is the possibility of nucleation and growth from a transient ordered phase. This idea goes back to Ostwald's "rule of stages"[14] and has been discussed at length regarding polymers, especially polyethylene, by Keller and collaborators.[15−19] The basic argument is that if a second ordered phase has a low nucleation barrier, then it will be the first to nucleate, even if it is not the thermodynamically stable one. The examples include crystallization from the hexagonal phase of polyethylene (which is stable at high pressure and only metastable at atmospheric pressure) and its subsequent transformation to the stable orthorhombic form,[15−19] nucleation of a transient rotator phase in low molecular weight even-*n* alkanes followed by the transformation to the stable triclinic phase[20,21] and nucleation of a transient rotator phase in *n*-alkane solutions with subsequent transformation to the stable orthorhombic crystalline form.[20] It is not clear to us whether any of the systems mentioned earlier that exhibited the behavior of SAXS before WAXD in fact involves the initial nucleation from a metastable phase.

However, before one can ponder the origin of crystallization, there are some fundamental concerns about the experimental techniques being used. The difficulty in probing the early stages of crystallization is the weak signals from the small volume fraction involved, combined with the detection limits of the various techniques such as SAXS and WAXD. Because the detection limits of SAXS and WAXD are different to detect the presence of initial crystalline phase, merely comparing the first appearance of SAXS and WAXD intensities may not provide meaningful information. It has been argued that since the crystallinity in the early stages is low, the WAXD technique may not be able to detect it. By contrast, the lower fraction of crystallinity can be readily detectable by SAXS as long as the contrast between the constituting phases is sufficient and the length scale is within the detectable range (less than 100 nm). For example, the SAXS technique has been routinely used to measure low concentrations of samples in solutions, such as proteins with concentrations as low as 0.3%.[22]

In this study, our first objective was to confirm the ability of WAXD to quantitatively determine the detectable crystallinity (detection limit). This information is not available in the literature. For this purpose, solutions of *n*-paraffin ($C_{33}H_{68}$) in dodecane ($C_{12}H_{26}$) in varying concentrations were prepared which simulated different degrees of crystallinity in polymer (polyethylene). A modeling approach was also used to calculate the WAXD profiles to address the effect of crystal size at low crystallinity. An excellent agreement has been obtained between the expected crystallinity and the detection limit, which is described in the Appendix.

The main part of this study was focused on the early stages of isothermal melt crystallization in a fractionated *i*PP sample. This material was chosen on the basis of the recent study of the same polymer by Ryan et al.[11,12] In addition to simultaneous SAXS and WAXD measurements, the early stages of polymer crystallization were also followed by light scattering (LS), which detected the evolution of anisotropic structures in the crystallizing polymer melt. Recently, the early stages of crystallization in PET from the glassy state and in *i*PP from the molten state were also investigated by time-resolved laser light scattering.[23,24] These reports indicated that large domains of density fluctuations started to increase first, whereby birefringence developed later after a time lag. In this study, time-resolved light scattering was performed separately from simultaneous SAXS and WAXD measurements. The three techniques were not carried out simultaneously because LS commanded the sample thickness to be about 10 μm to avoid multiple scattering, while SAXS and WAXD required the sample thickness to be about 1.5 mm for best signal resolution.

Expectation of Induction Period. As we study the morphological features developed during the period prior to the observation of crystallization (termed "induction period"), it is necessary to outline the expectation of this period on the basis of classical nucleation and growth theories and then to explore the alternatives. The first question one can ask is whether the experimental data exhibit any deviation from a simple model of nucleation and growth. We will discuss what is "expected" from the classic nucleation theory and how experimental observations may manifest themselves.

The experiment under consideration is ideally an instantaneous "quench" from a temperature above the equilibrium melting point ($T > T_m^o$) to a temperature below. Clearly, experimentally this cannot be instantaneous, and the removal of heat from the sample will cause a finite time to actually reach the desired temperature. This time is, in some sense, the limit on the resolution of the experiment in the temporal domain. The classical picture of nucleation is that at time $t = 0$ the system is the liquid phase in a metastable equilibrium at temperature $T < T_m^o$. The molecules, by random diffusion, are sampling the ensemble of possible configurations and packing. For a crystal to be able to grow, the random rearranging must sample a cluster with the crystalline structure of a critical size. This "critical nucleus" is the size such that its free energy will decrease with subsequent growth, because of the competition between the costly interfacial energy and the bulk driving force. Since the liquid is in a metastable equilibrium, there will be a temporally constant nucleation rate.

Upon quenching from $T > T_m^o$ to $T < T_m^o$, one can ask how long it will take for the liquid to relax from its structural and thermal properties of the liquid at higher temperature to those associated with the metastable liquid at the lower temperature (assuming instantaneous removal of the heat). This relaxation time could cause a delay in the initiation of nucleation. For systems under consideration here, far from their glass transition, there has been no evidence for, and no reason to expect,

long relaxation due to temperature changes. The system should relax in ≪1 s, and such an induction time can be negligible. This kind of induction time has only been manifest in systems below or very near their glass transition where the system falls out of equilibrium on time scales of the measurement, and thus relaxation is not extremely fast (i.e., cold crystallization of polymers).[3−8] If there were such an induction time, one would expect it to increase with increased quench depth, due to both a larger change in properties associated with a deeper quench and a slower relaxation due to a lower temperature.

Induction times can also be manifest by an experimental artifact. As every experimental technique has its sensitivity and detection limitation due to statistics and noise, an experimentally determined induction time is not the time when crystallinity exceeds zero, but rather when it exceeds some finite fraction, which will be set by the specific measurement. Thus, to understand how classical nucleation and growth may manifest itself in such an experiment, we need to consider how nucleation and growth are expected to proceed. If we consider a situation where only nucleation is measured, as in the emulsion droplet experiments, the nucleation rate is a constant in time, and thus the scattered intensity increases (initially) linearly from time $t = 0$, without any induction time.[29] The simplest nucleation and growth theory can be embodied in the Avrami equation:[25−29]

$$X_t = 1 - \exp(-K((t - t_0)/\tau)^n) \qquad (1)$$

where X_t is the relative degree of crystallinity by volume, K is a constant containing the nucleation and growth parameters, t_0 is the induction time, τ is a time constant, and n is the Avrami exponent depending on the mechanism of nucleation and the form of crystal growth. The Avrami equation in its early time limit provides an integration of the total crystallinity (relative) combining a constant nucleation rate with growth. This leads to a single rate constant that is the product of nucleation and growth rates and an exponent that must be >1 and is related to the dimensionality of the growth. While the Avrami formalism has "issues" surrounding its form at late times when saturation occurs, and questions surrounding the exact effective dimensionality of the growth and the exponent, it works well in the early (as early as can be measured) and intermediate times. If we expect a metric of the crystallinity to evolve in time, from $t = t_0$ with a power of 2 or 3 for example, then it is not correct to try to use a linear extrapolation in time to zero crystallinity, to determine a meaningful induction time (or onset time).

The crystallinity expected from this classical model can take on different appearances depending on how it is plotted. Using an Avrami exponent (n) of 2.5 and three time constants (τ), we plot the crystallinity on a linear y-axis with a logarithmic time axis in Figure 1a (where $t_0 = 0$ is the time of the quench). It is clear from eq 1 that these curves have the same induction time ($t_0 = 0$); however, this cannot be determined from the data plotted in this way since plotting on a log t-axis creates a false impression that different onset times exist. The time to reach, say 50% crystallinity, does relate closely to the time constant, and thus different τ causes a horizontal "shift" on this type of plot. In Figure 1b, the same values are plotted on log−log axes. Here the initial

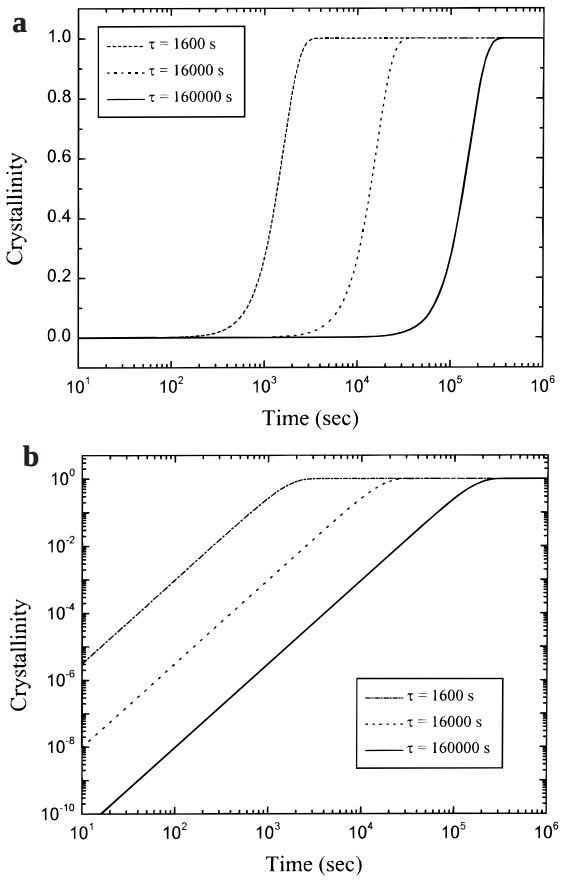

Figure 1. Crystallinity from Avrami equation with different time constants, τ, on (a) a linear y-axis with a logarithmic time axis and (b) a logarithmic y-axis with a logarithmic time axis (where $t = 0$ is the time of the quench).

stage shows a linear behavior in all three curves, and the slope of the curves (before saturation) yields the exponent. Again, all three curves share a common induction time of $t_0 = 0$. The log−log plot thus is particularly sensitive to detect the deviation of the Avrami behavior in the early stages of crystallization.

To see the effect of experimental sensitivity on such a simple Avrami form, we plot (Figure 2a) the log−log curve for $\tau = 16\,000$ s with three varying degrees of noise: 1%, 0.1%, and 0.01%. As can be seen, the lower the noise level (i.e., the better sensitivity), the earlier in time will the data lie on the ideal curve before becoming dominated by the noise. Such data are sometimes presented on linear axes. To see the effect of noise on such data, we plot the two curves of Figure 2a on linear axes in parts b and c. In these two figures, the solid curve is the ideal curve before the random noise was added. The dashed lines are guides to the eye, whose intersection represents the "onset time" which would be determined using an interception method. This "onset time" is also close to the time at which the signal rises above the noise. As can be seen from parts b and c of Figure 2, the two different noise levels depicted here would yield onset times of 350 and 2000 s, respectively, for the same crystallization process, which in reality has zero induction time. It is clear that an induction time cannot be separately determined from such measurements in the absence of a particular model.

We will therefore present the data in this study as though nucleation and growth were happening according to classical nucleation and growth theory of a single-

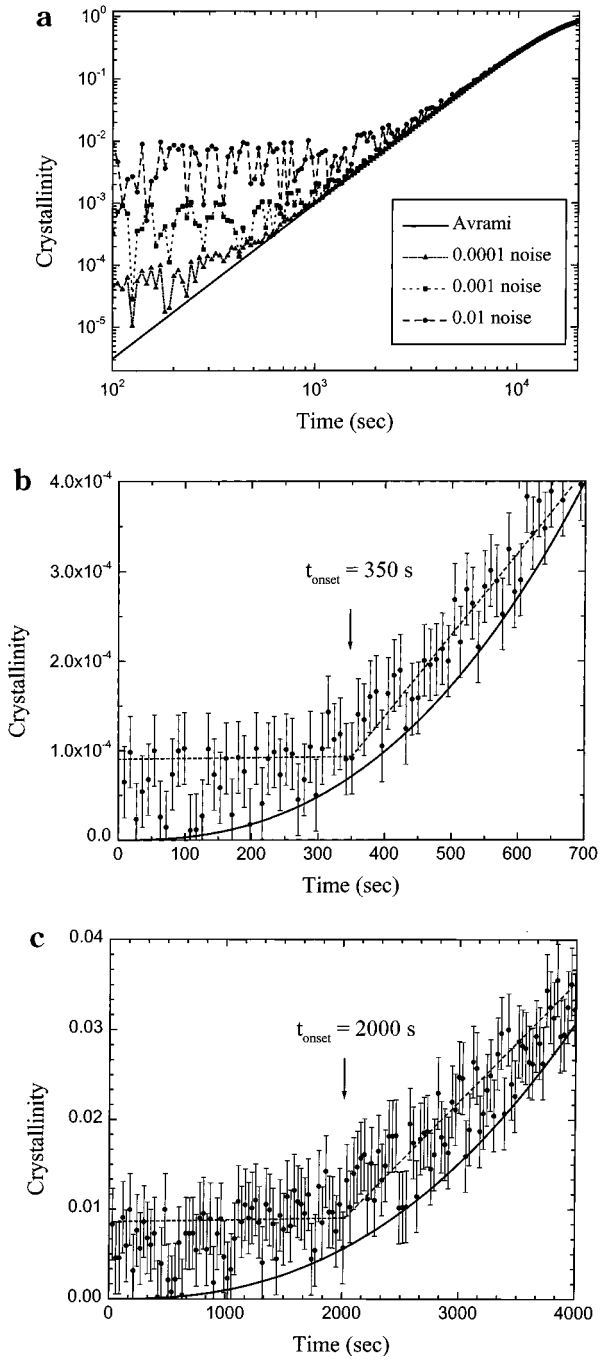

Figure 2. Crystallinity from Avrami equation with (a) τ = 16 000 s and three varying degrees of noise, 1%, 0.1%, and 0.01%, to demonstrate the effect of experimental sensitivity on the functional form on log−log scales; (b) τ = 16 000 s and degree of noise 0.01% on linear scales; (c) τ = 16 000 s and degree of noise 1% on linear scales.

crystal phase from the liquid and see whether there are any deviations from such a model.

Experimental Section

Samples and Preparation. The fractionated metallocene-based isotatic polypropylene (*i*PP) sample was supplied by Exxon Chemical Co. The sample had number- and weight-average molecular weights, M_n and M_w, of 41 800 and 87 300, respectively, and a polydispersity (M_w/M_n) of 2.09 with total defects (mole percent) of 1.11. The extrapolated equilibrium melting point, T_m^o, of *i*PP from DSC measurements was 189 °C. The sample was molded into void-free disks (7 mm in diameter) with thicknesses of 1.5 mm for X-ray measurements and melt pressed (at 195 °C) into thin films with thicknesses about 10 μm for light scattering study.

Characterization Techniques. Simultaneous SAXS and WAXD measurements were carried out at the Advanced Polymers Beamline (X27C, λ = 1.307 Å) in the National Synchrotron Light Source (NSLS), Brookhaven National Laboratory (BNL). The details of the experimental setup at the X27C beamline have been reported elsewhere.[30] Two linear position-sensitive detectors (European Molecular Biological Laboratory, EMBL) were used to detect the simultaneous SAXS and WAXD signals. The sample-to-detector distance for the SAXS detection was 990 mm and for the WAXD detection was 100 mm. The scattering data from silver behenate and duck tendon were used to calibrate the SAXS profile, and a silicon standard was used to calibrate the WAXD profile.

Isothermal melt crystallization was performed using a "dual-chamber temperature jump" apparatus, which has been described previously.[31] The sample was first equilibrated at 195 °C for 5 min and then pneumatically "jumped" to the lower temperature chamber for time-resolved simultaneous SAXS and WAXD measurements. In this study, three isothermal crystallization temperatures, T_c's, were chosen: 145.0, 143.0, and 137.0 °C. Note that the crystallization temperature of 145.0 °C for *i*PP ($\Delta T = T_m^o - T_c = 44$ °C) is relatively shallow, which resulted in a considerably long "induction time" during the measurement (about 2000 s). The time to reach the equilibrium measurement temperature after the temperature jumping was less than 150 s. The initial 90% of the temperature change occurred at a rate about 300 °C/min. At thermal equilibrium, temperature fluctuations were less than ±0.3 °C. The data acquisition time for the X-ray measurement was 20 s per scan, with a pause time of 5 s between adjacent scans. The total data collection time was 3−4 h except for the isothermal crystallization at T_c of 137.0 °C (∼1 h).

The same "dual-chamber temperature jump" apparatus was also used in the laser light scattering measurement. In the experimental setup, a polarized He−Ne gas laser with a wavelength of 632.8 nm and a one-dimensional photodiode array detector (EG&G PARC model 1422) having a resolution of 1024 pixels (pixel size 25 μm) were used. The sample-to-detector distance was 84 mm, which covered a q range from 0 to 0.0027 nm^{-1} ($q = (4\pi/\lambda) \sin\theta$, with 2θ being the scattering angle). The data collection time per scan was either 20 or 10 s per frame, depending on the chosen crystallization temperature. Only the H_v geometry was used for the measurement; i.e., the optical axis of the analyzer was set perpendicular to that of the polarizer. The experimental procedures in the light scattering measurements were identical to those used in the simultaneous SAXS and WAXD measurements. Five isothermal crystallization temperatures were chosen: 144.4, 141.3, 139.3, 135.9, and 132.6 °C.

Data Analysis

SAXS. Proper analysis of the SAXS data depends on the state of structure in the materials. Since we know little about the early stages of crystallization, the scattering data collected at the early stages of crystallization must be considered by different methods, based on different models of morphology. These methods are summarized as follows. If the detected scattering profile is diffuse, the data can be analyzed with (1) the Guinier plot assuming that the scatterers are individual nuclei which are formed at low concentrations and noncorrelated with each other, (2) the Debye−Bueche approach assuming that the scattering is due to random two-phase fluctuations with sharp interface between the phases,[32] or (3) the single particle scattering analysis assuming that nuclei are formed in higher concentration but are noncorrelated.[33] If the scattering profile exhibits a discrete peak, the data may be analyzed according to (4) the Cahn−Hilliard theory[9,10] assuming that the scattering maximum possesses the characteristics of

spinodal decomposition, i.e., the peak intensity increases exponentially with time but the peak position remains constant, or (5) the correlation function analysis assuming that the peak arises from finite lamellar stacks.[33−35] In the Results and Discussion section, the scattering data collected at the early stages of crystallization were considered with all of the above methods. The detailed analysis for methods in (1)−(5) can be found in the textbook or the references cited above. In the later sections, we will describe the physical meaning and only the analysis schemes of the different SAXS variables used.

WAXD. From the WAXD profile, the peak position, peak height, peak width, and integrated intensity for each crystal reflection and amorphous background can be extracted. In this study, the deconvolution procedures were carried out using a custom code capable of dealing with time-resolved spectra. A Gaussian peak riding on a polynomial was used to describe the amorphous background. All other reflection peaks were also fitted with Gaussian functions. By dividing the total intensities of the crystalline reflections I_c to the overall intensity I_{total}, a measure of the mass fraction of the crystalline phase in the sample can be obtained. This value is termed as the apparent mass degree of crystallinity, ϕ_{mc}. Because of possible defects in the crystal lattice and thermal disorder, the measured value of ϕ_{mc} will be lower than the true value. The measured mass crystallinity is related to the true volume degree of crystallinity, ϕ_{vc}, as $\phi_{mc} = f(T)\phi_{vc}$, where $f(T)$ is a temperature-dependent factor taking into account of the deviations mentioned above and the correction for translating mass to volume. We note that by using this deconvolution method the sample is assumed to possess two ideal phases (α-form crystalline and amorphous), which is the criterion to define the term "crystallinity".[32] Ordering into another crystalline or mesomorphic form would not be included in this metric of crystallinity.

Since the crystal reflection signals were extremely weak in the early stages of crystallization, the following strategy was used to estimate the crystallinity from the initial WAXD profiles. As four diffraction peaks (110), (040), (130), and (−131) were detected by WAXD, the fitting for each peak in the measured profile was determined by the signal-to-noise ratio as well as the tolerance of the fit. It was found that the area ratios between the different peaks were about constant in all diffraction patterns. Thus, as some of the peaks became too weak to be resolved by the curve fitting method, the contribution of the remaining peaks was scaled to account for the assumed relative intensity of the weakest peaks. This is consistent with analyzing the data in terms of growth in the stable α-modification. The determination of the crystallinity was stopped and considered too weak to be quantitatively determined when fewer than two of the four crystal reflections could be isolated. Using this procedure, we have estimated that the minimum measurable crystallinity in the time-resolved study was about 2%, which is in good agreement with the method listed in the Appendix (1%). The poorer statistics in the time-resolved study is due to the fact that the intensity of iPP is rather equally distributed among four peaks and raises the minimum measurable crystallinity to 2%, while in the *n*-alkanes the scattering from the crystalline reflections is contained in two peaks, one much stronger than the other (the measurable crystallinity is 1%).

Light Scattering. In polarized light scattering measurements, the intensity collected under the H_v condition can be analyzed to reveal information on particles with orientational order (birefringence) or orientation fluctuations whereas the V_v data (the polarizer and the analyzer parallel to each other) are related to the combination of orientation and density fluctuations. The detailed relationship between the H_v and V_v intensities can be found elsewhere.[36] As we only collect the scattering intensity under the H_v condition, I_{H_v}, we will briefly describe how the data can be analyzed. The angular distributions of I_{H_v} can be described as[36]

$$I_{H_v} \propto \langle \delta^2 \rangle \int_0^\infty f(r) \frac{\sin(qr)}{qr} 4\pi r^2 \, dr \qquad (2)$$

where $\langle \delta^2 \rangle$ is the mean-square molecular anisotropy, and $f(r)$ is the correlation function of the orientational distribution in an optical axis. If the correlation function $f(r)$ has a simple exponential form ($f(r) = \exp(-r/\xi)$ with ξ being the correlation length) as proposed by Debye et al.,[37,38] then the scattering intensity can be rewritten as

$$I_{H_v}(q) = A\left(\frac{1}{1 + \xi^2 q^2}\right)^2 \qquad (3)$$

where A is a constant. This is the basis for the Debye−Bueche approach. If we plot $[I_{H_v}(q)]^{-1/2}$ versus q^2 and determine the slope and the intercept, then the correlation length ζ can be calculated as the value of (slope/intercept)$^{1/2}$. To discuss the crystallization development, it is convenient to define the integrated scattering intensity A_{H_v} as follows:

$$A_{H_v} = \int_{q_1}^{q_2} I_{H_v}(q) \, dq \qquad (4)$$

where q_1 and q_2 are defined by the range of the data collected. The value of A_{H_v} thus is proportional to the volume fraction of the orientational anisotropy between the two constituting phases.

Results and Discussion

Evaluation of Simultaneous SAXS and WAXD Results during Isothermal Crystallization. Typical time-resolved SAXS and WAXD profiles obtained during isothermal crystallization of *i*PP film at 145.0 °C are shown in parts a and b of Figure 3, respectively. The low degree of supercooling (T_c = 145.0 °C, ΔT = 44 °C) resulted in a slow crystallization rate, allowing the detailed examination of simultaneously collected SAXS and WAXD profiles. Selected time-resolved SAXS and WAXD profiles at 145.0 °C are shown in parts a and b of Figure 4, respectively. It is seen that a detectable scattering shoulder first appears in the raw SAXS profile (marked by a thicker line) at 3005 s (<1 h), and the crystalline reflections first become identifiable at about 4255 s (also marked by a thicker line). The determination of the initial SAXS peak here was based on the signal-to-noise evaluation (S/N ≈ 2) at the scattering maximum (q = 0.02 Å^{-1}), and that of the WAXD profile was based on two positive determinations (S/N ≥ 2) of the four strong reflections (110), (040), (130), and (−131) by the fitting routine. We term this method as the S/N method. The time difference between the observation of the first SAXS peak (3005 s) and the initial WAXD crystal peaks (4255 s) is quite significant

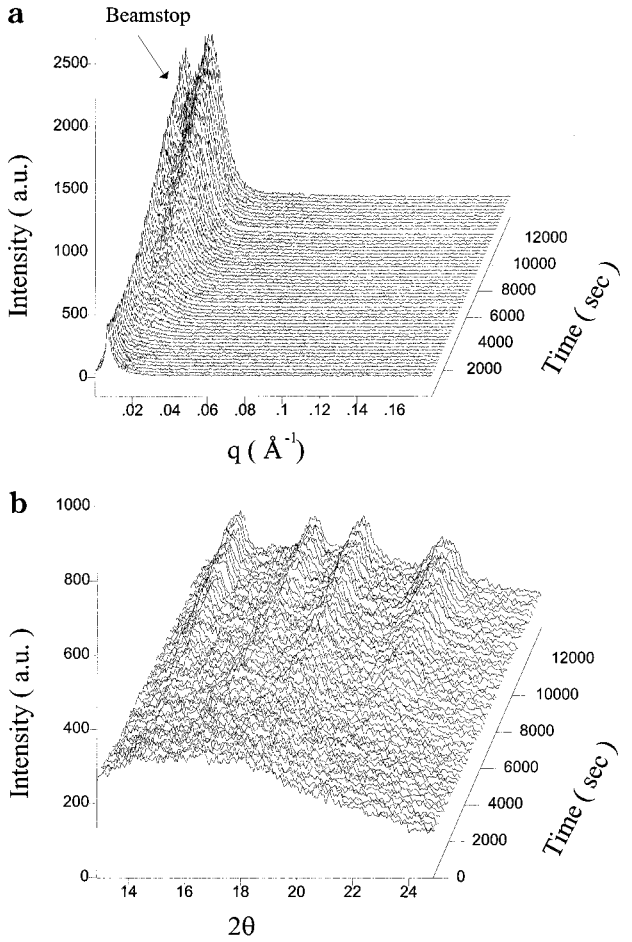

Figure 3. Simultaneous (a) SAXS and (b) WAXD profiles collected during isothermal crystallization of *i*PP at 145.0 °C for 3 h.

(1250 s). This is in agreement with the observations by Ryan et al., who have also studied the system of *i*PP with a much higher molecular weight (M_w = 520 000) and a broader polydispersity (M_w/M_n = 4).[11]

As Ryan et al. have used the interception method to determine the onset time for the initial peak appearance, we have also compared the S/N method with the interception method. The time evolution profiles of both the invariant Q (eq 5)[33,35] and the integrated intensity I_{int} (eq 6) within the experimental q range (q_1 = 0.0075 and q_2 = 0.20 Å^{-1}) from SAXS data of *i*PP at 145.0 °C are shown in Figure 5 (in linear scales).

$$Q = \int_0^\infty I(q)q^2\,\mathrm{d}q \propto \phi_a\phi_c(\rho_c - \rho_a)^2 \qquad (5)$$

$$I_{int} = \int_{q_1}^{q_2} I(q)\,\mathrm{d}q \qquad (6)$$

In eq 5, the invariant Q is proportional to the product of volume fractions for the crystalline and amorphous phases (ϕ_c, ϕ_a) and the scattering contrast due to the electron density difference $(\rho_c - \rho_a)^2$. It is found that the onset times for both Q and I_{int} are about the same, which is also similar to the time determined from the signal-to-noise evaluation at q = 0.02 Å^{-1}. As shown earlier, such determined onset times (termed apparent onset times) are not fundamental, a point which we will return to in the discussion later. However, for the purpose of comparison, we will continuously use the interception method to analyze the WAXD and light scattering data.

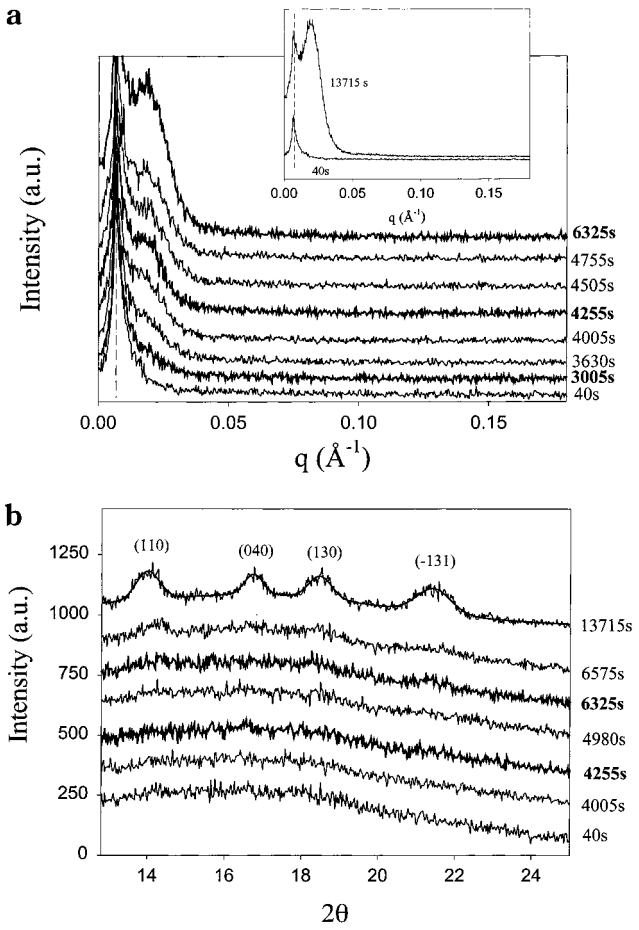

Figure 4. Selected (a) SAXS and (b) WAXD profiles collected during isothermal crystallization of *i*PP at 145.0 °C for the comparison of the initial appearance of the SAXS peak and the WAXD crystal reflections.

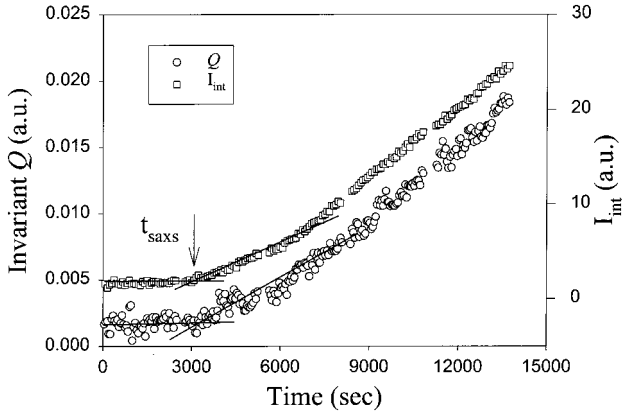

Figure 5. Time evolution of the invariant Q and the integrated intensity I_{int} from the SAXS data during isothermal crystallization of *i*PP at 145.0 °C. The apparent onset time (t_{SAXS}) is determined using an interception method.

The comparisons of the crystallinity ϕ_{mc} obtained from the deconvolution analysis of the WAXD data and the invariant Q from the SAXS data are made in parts a and b of Figure 6 at 145.0 and 143.0 °C, respectively. The development of the crystallinity appears to consistently lag behind the invariant Q. The period of the time lag is indicated by two dotted lines, which represent the apparent onset time for the initial appearance of the SAXS peak (t_{SAXS}) and the apparent onset time for the minimum measurable crystallinity from the crystal reflections in WAXD (t'_{WAXD}) using the method men-

tioned in the Data Analysis section. The value of t'_{WAXD} is larger than the apparent onset time for the initial appearance of the WAXD peak (t_{WAXD}). This is because that the determination of the crystallinity was stopped as the signals were too weak to be quantitatively determined when fewer than two of the four crystal reflections could be resolved by the curve-fitting method, while the initial appearance of four crystal reflections could still be identified to a shorter time. In this paper, we intend to use t_{WAXD} rather than t'_{WAXD} as the onset time for WAXD analysis. It is found that the lag time ($t_{WAXD} - t_{SAXS}$) decreases with decrease in crystallization temperature or increase in the degree of supercooling. These results are consistent with the data reported by Ryan et al.[11]

Analysis of the SAXS Data in the Induction Period. The "induction period" referred to here was defined as the period between the starting time of the measurement (t_0) and the nominal onset time for WAXD (t_{WAXD}). This period is associated with the characteristic time to grow crystals (α-form) from the amorphous state to the level of detectable crystallinity. This time increases with increased crystallization temperature. By definition, no excess SAXS profile was measurable prior to t_{SAXS}. (This is consistent with Figure 5 that the values of Q and I_{int} are constant before t_{SAXS}.) After the time t_{SAXS}, a discrete scattering maximum was seen in the measured profile, whose intensity increased dramatically with time (Figure 4a). As the intensity of the scattering maximum increased, the low-angle intensity uptake near the beam stop also increased at about the same rate. Since a SAXS peak at finite q was observed during the "induction period", we feel that the Guinier approach (method 1), the Debye−Bueche approach (method 2), and the single lamellae particle scattering (method 3) are not appropriate for the analysis of these data.

Discrete scattering profiles observed during the period between t_{SAXS} and t_{WAXD} have also been reported by Ryan et al.[11,12] They have used the method of spinodal decomposition to analyze their SAXS data since the peak intensity grew exponentially with time, while the peak position remained constant. This behavior was considered to be characteristic of spinodal decomposition at the early and the intermediate stages of crystallization. At the late stage of the decomposition, the domains would continuously coarsen with time, shifting the peak position to lower values of q. However, in this study, detailed examination of the SAXS profiles collected in the induction period revealed a different behavior. It was found that despite the increase in scattering intensity, the scattering peak position was not shifted to lower q values even at long times. At very early times the data even suggested a slight increase in q (with time), indicating a decrease of the correlation length or the long period. In Figure 7, two types of long periods are depicted: (a) one directly calculated from Bragg's law, L_b (= $2\pi/q_{max}$, where q_{max} represents the peak position in the Lorentz corrected scattering plot, i.e., Iq^2 vs q), and (b) one calculated using the correlation function ($\gamma(r)$, eq 7), L (= the distance in $\gamma(r)$ where the first maximum occurs). Even though the variations of these values are at the level of experimental uncertainty, a trend of slight decrease with time is suggested, which is consistent with early results from other polymers.[39−41] As a result, we feel that the analysis of spinodal-decomposition-like behavior is also not appropriate for the analysis of the data. It is seen that the Bragg long period L_b is always larger than the long period L from the correlation function. This has been a general phenomenon observed during crystallization of polymers[39−41] and can be attributed to the presence of a broad distribution in long period.[40] The final average long periods after isothermal crystallization at 145.0, 143.0, and 137.0 °C are 245, 235, and 208 Å, respectively.

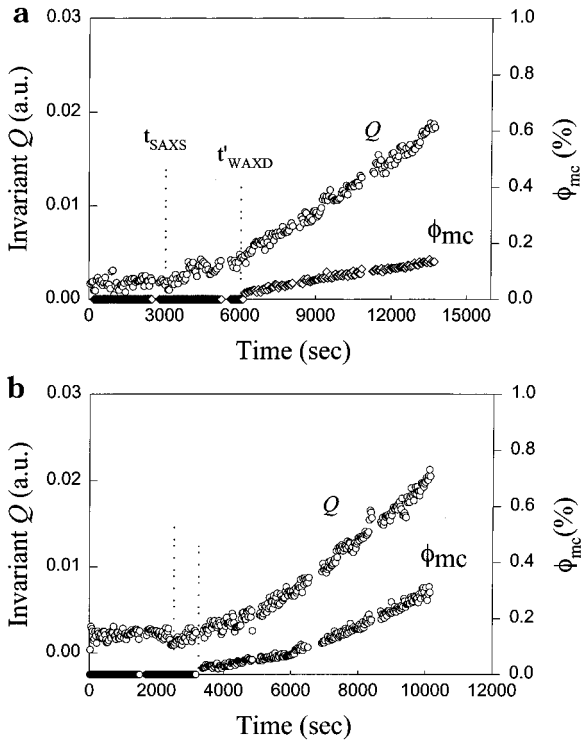

Figure 6. Time evolution of the invariant Q and crystallinity ϕ_{mc} during isothermal crystallization of *i*PP at (a) 145.0 °C and (b) 143.0 °C. The two dotted lines represent the values of t_{SAXS} and t'_{WAXD}.

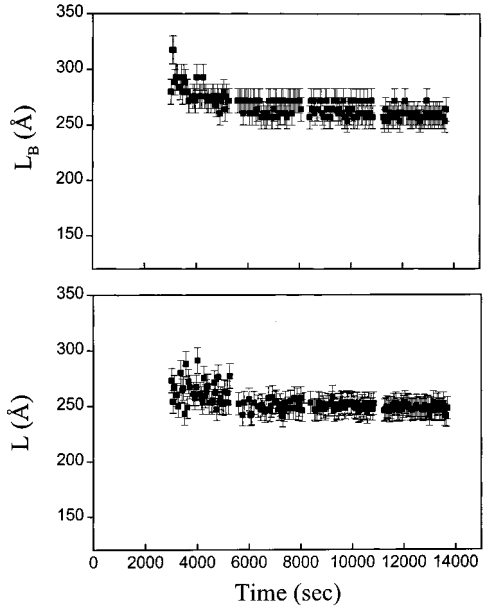

Figure 7. Time evolution of the morphological parameters: (a) long period from Bragg's law, L_b, and (b) long period from correlation function, L, during isothermal crystallization for *i*PP at 145.0 °C.

$$\gamma(r) = \int_0^\infty I(q)q^2 \cos(qr)\, dq \qquad (7)$$

The simplest explanation for the development of the scattering peak in the "induction period" is due to the formation of a finite lamellar structure. In this case, the position of the peak is related to the long period between the two adjacent lamellae. This argument appears to be credible as semicrystalline *i*PP samples always show a crystal lamellar structure in the morphology. In the "induction period", if one of the lamellar phases represents the crystalline phase, then the concentration of the lamellar structure must be low such that the total crystallinity is less than the WAXD detection limit. Since SAXS has a lower detection limit, the earlier detection of the SAXS signal is quite reasonable.

Light Scattering during Isothermal Crystallization. Time-resolved light scattering experiments in the H_v mode was also carried out separately to follow the early stages of crystallization in *i*PP at different temperatures. As the initial scattering patterns during crystallization were completely isotropic (the four-leaf clover pattern was observed only in the later stages of crystallization), the detector axis was placed perpendicular to the axis of the analyzer for measurement. It was seen that during the early stages of crystallization the scattered intensity decreased monotonically with the scattering angle. The time evolution of the integrated intensity A_{H_v} (using eq 4) for *i*PP is shown in Figure 8a. The apparent onset time when A_{H_v} starts to increase above background (t_{LS}, indicated by the arrow) can also be estimated from these (linear) plots. The value of t_{LS} thus indicates the time when the birefringence is first detected in the melt. To estimate the average size of these ordering domains, the Debye−Bueche approach was applied to analyze the H_v excess scattered data (after the subtraction of the scattered intensity from the initial melt) within the period between t_{LS} and t_{WAXD}. The correlation length ξ obtained by eq 3 is shown in Figure 8b. It is seen that the correlation length increases with time and temperature from 300 to 1800 nm in the "induction period", which is in good agreement with an earlier light scattering report[24] and the recent results of the early stages of crystallization in *i*PP reported by Winter et al.[42,43]

A comparison of the three onset times determined by different scattering techniques is shown in Figure 9. It is interesting to see that, at a given temperature, the following order always exists: $t_{WAXD} > t_{SAXS} > t_{LS}$. This indicates that large birefringent objects (by LS) are detected in the melt before the detection of lamellar structure by SAXS. In other words, domains with detectable mean-squared anisotropy by light scattering are formed in the "induction period", where sizes are comparable with the laser light wavelength. This is not surprising since light scattering can be sensitive to detect a much smaller volume fraction ($\sim 10^{-5}$) and, as we show below, the apparent delay in the SAXS can be attributed to its lesser detection limit (~0.1%), and the WAXD techniques clearly has the poorest detection limit (~1%). We note that the V_v mode of the small-angle light scattering was not carried out in this study. As the V_v mode detects both fluctuations from orientational anisotropy and density, its detection limit may be even lower than the H_v mode. If the V_v experiment was carried out, it would not be surprising that the induction time from V_v can be shorter than H_v.

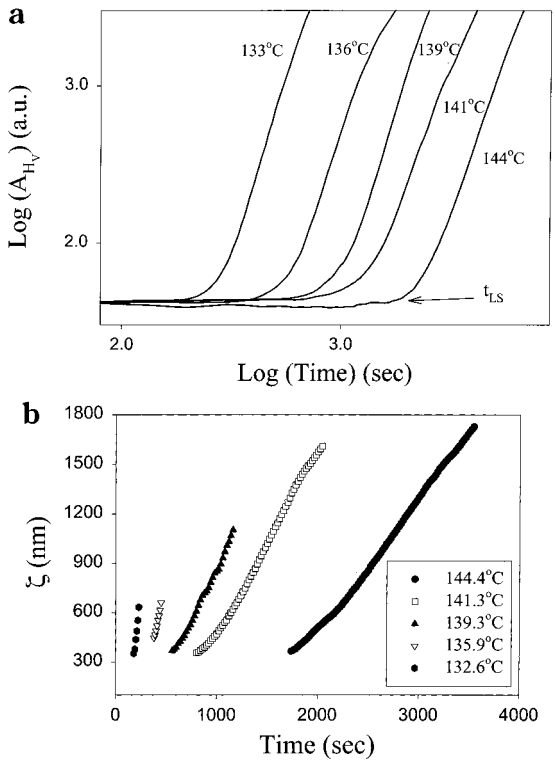

Figure 8. Changes of (a) the integrated light scattering intensity and (b) the correlation length for *i*PP during isothermal crystallization at different temperatures. The arrow in (a) indicates the value of the apparent onset time for light scattering, t_{LS}.

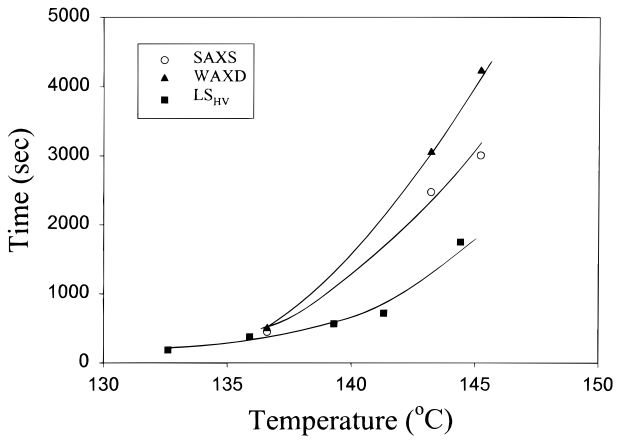

Figure 9. Comparison of the apparent onset time for SAXS, WAXD, and LS for *i*PP at different crystallization temperatures.

Possible Mechanism in the Early Stages of Crystallization. We have shown that WAXD can give us an absolute measure of the crystallinity (in mass) of the sample. The detection limits of LS and SAXS are not easily independently determined; however, it is well-known that LS can detect a smaller volume fraction than SAXS, and SAXS can detect a smaller volume fraction than WAXD, if the objects or spacings are in the right length scale range. In the following, we assume that the process of crystallization is classical nucleation and growth. Our objective is to see whether simple scaling of SAXS and LS data corresponds to the WAXD crystallinity.

While LS and SAXS (as performed here) do not allow an absolute determination of the volume fraction of the birefringent or denser phase (i.e., volume crystallinity

in the two-phase approximation), we can make some approximations. As the laser light will scatter coherently from an object, the intensity will be proportional to the square of its volume. Since it is the largest growing particles that will contribute most to the integrated intensity (as opposed to the small, newly nucleated ones), it is reasonable to assume that the crystal volume fraction is proportional to the square root of the intensity. This approximation should be good as long as the total crystallinity is low and the particles do not interact with each other. These particles should be thought of as a superstructure, such as, but not necessarily, spherulites. When they begin to interact, the intensity will fall below this ideal level. Since there is a finite background intensity at early times, that value must be subtracted off as well. The only free parameter to relate the LS integrated intensity to the crystallinity is a constant. Thus, the "crystallinity" determined from LS has the following relationship:

$$X_{LS} \propto (\text{integrated intensity} - \text{background})^{1/2} \quad (8)$$

Since the lamellae only have very short-range correlation (such that the lamellae peak is much broader than the X-ray resolution), the integrated intensity from SAXS should be linearly proportional to the crystallinity. This approximation too may break down when the primary crystallization is complete, and interlamellar regions may try to crystallize. However, in the early stages, the approximation is quite reasonable. Again, the initial time background should also be subtracted. Here, we choose to use the integrated intensity instead of the invariant (Figure 5), since it has better statistics, and since the peak position does not change much, they track each other. Again, there is only a single free parameter, the scaling constant. Thus, the "crystallinity" determined from the SAXS is

$$X_{SAXS} \propto \text{integrated intensity} - \text{background} \quad (9)$$

The WAXD is analyzed as discussed above and yields absolute crystallinity values (converted to volume fraction). We also consider an Avrami form for the crystallinity with an exponent of 2.5 consistent with the data of Kim and Kim[44] and Pogodina and Winter.[42,43] The time constant, which will depend on temperature, is the only free parameter necessary to make this form fit the data. The Avrami crystallinity (in volume) considered here has the form $X_{AVRAMI} = 1 - \exp(-(t/26500)^{2.5})$. Plotted in Figure 10a (the log−log plot) are the WAXD crystallinity, the SAXS crystallinity X_{SAXS}, and the LS crystallinity X_{LS}, and the Avrami form X_{AVRAMI} at 145.0 °C. (In Figure 10, the relative values of volume crystallinity for LS, SAXS, and Avrami modeling are scaled separately on the basis of the measured crystallinity from WAXD.) The actual limits of detection here with data analyzed in this way are 2% for WAXD (the lowest points where finite crystallinity could be extracted), ~0.8% for SAXS, and 0.1% for LS limited by the background. These independently determined values except for WAXD are not absolute, but rather are linearly scaled based on the assumptions of the classical nucleation model.

The LS data in Figure 10a match the Avrami form only at earlier times but then begin to fall lower than the Avrami prediction at crystallinities of a few percent. This is not surprising, as this is when the growing objects may begin to interact with each other, causing

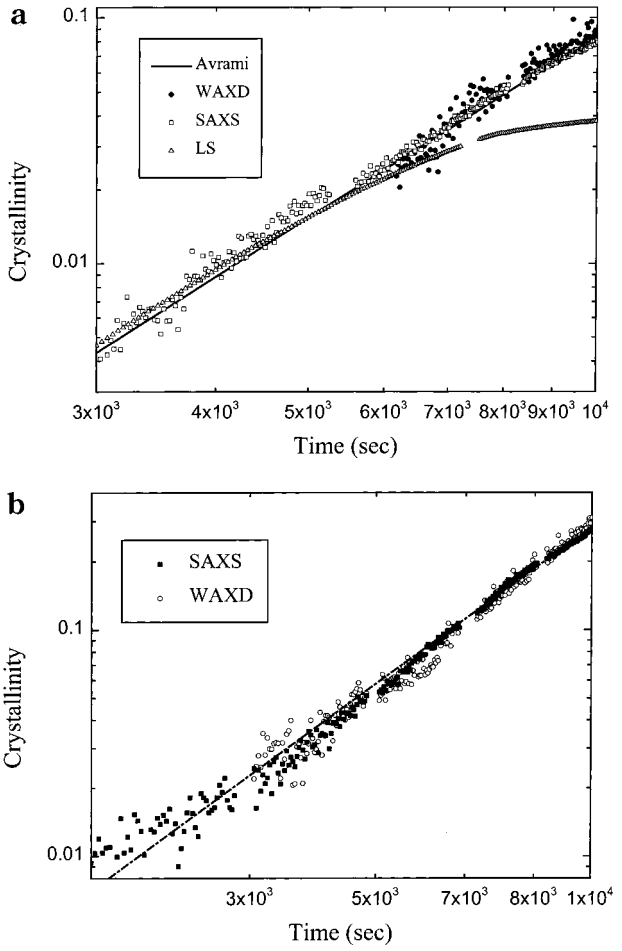

Figure 10. Time evolution of relative crystallinity from WAXD, SAXS, LS, and Avrami form for iPP at (a) 145.0 °C and (b) 143.0 °C.

the breakdown of the approximation relating the scattering intensity to the volume crystallinity. This behavior is consistent with the report of gelation at the early stages of crystallization.[42,43] The SAXS data follow the Avrami form over the whole range of times shown here and become limited by noise at the early times. The WAXD data also follow the Avrami curve, similar to SAXS and the extrapolation of LS after its detection limit at 6100 s. Figure 10b shows the similar isothermal crystallization behavior at 143.0 °C. In this figure, only the data from SAXS and WAXD are shown (since the LS was not acquired at the same temperature).

The experimental results presented here are consistent with the following hypothetical sequence during isothermal crystallization.

(1) Primary nucleation occurs in the form of a critical nucleus of an ordered phase. It may be the "mesophase" with no detectable crystallinity which has been observed to be "long-lived metastable" on quenching iPP.[45] The ordered phase may grow in the typical lamellar mode with an average lamellar spacing. At this point only a few such crystallites are present, and the LS, SAXS, and WAXD signals are below the detection limits. The total crystalline fraction may be following the Avrami form, which is exponentially small at early times and grows linearly, on a log−log scale. (Here we are far from the saturation effect at long time.) At this stage, nothing is observable.

(2) The lamellar crystallites of the crystal phase grow in the form of superstructures, such as, but not neces-

sarily, spherulites. The superstructure particles grow in size with time, and new ones may appear. With a very low total crystalline fraction, the first thing we can detect is the LS signal. Here there may be relatively few such particles with a volume fraction of $\ll 10^{-3}$. These superstructure particles contain lamellae of a crystalline phase, but their volume fraction is below the detection limit of SAXS or WAXD.

(3) As the spherulites grow and new ones appear and the LS intensity continues to increase, the LS will be dominated by the large particles, and the data show an increase in size with time. Since light is coherent over the particles and the scattering is dominated by the growing of the large particles, not the appearance of small new ones, the total intensity scattered is proportional to the square of the particle size. The total crystalline fraction can thus be approximated by the square root of the integrated intensity. Thus, the LS intensity and ξ increase in this regime.

(4) The particles contain lamellae that are comprised of the crystal phase. As the total volume fraction increases, the SAXS detection limit is exceeded and the lamellar structure can be detected. Since the lamellae do not have long-range coherence over a superstructure particle, but are just a result of short-range stacking order, the SAXS intensity can be approximated as being linearly proportional to the fraction crystallized.

(5) The volume fraction of the crystalline phase is growing in the form of lamellae inside superstructures. In this regime, WAXD crystallinity becomes measurable and is the level anticipated on the basis of the SAXS intensity growth.

(6) Crystal growth continues in the α-form, increasing the intensities of LS, SAXS, and WAXD. The LS intensity will begin to level off much earlier than the others, more associated with the initial impingement of spherulites (at the gelation temperature) than the saturation of crystallinity.

Conclusions

Simultaneous synchrotron small-angle X-ray scattering and wide-angle X-ray diffraction and polarized light scattering measurements were performed to investigate the early stages of polymer melt crystallization in fractionated isotatic polypropylene (*i*PP). As the crystallinity during the early stages was very low, we first addressed the issue of detection limit for the WAXD technique. By using the solutions of *n*-paraffin ($C_{33}H_{68}$) in dodecane ($C_{12}H_{26}$) with different concentration (as low as 1%), we simulated polymers with varying degrees of crystallintiy. A modeling method was also applied to study the effect of crystal size on the detection of crystal reflections at low crystallinity. With these two methods, we conclude that the WAXD technique can detect crystallinity ~1% with crystal size as small as 20 nm. During the early stages of *i*PP isothermal crystallization, we found that peaks corresponding to a lamellar repeat from 20 to 24 nm were present in the supercooled melt (by SAXS) prior to the observation of three-dimensional crystal ordering of the α-form (by WAXD). In addition, we found that local orientational order (by polarized light scattering) with domain sizes about 300−900 nm were observable even before the detection of density fluctuations by SAXS. The size of the objects detected by light scattering increased with crystallization time and temperature. The behavior of the SAXS in the induction period for the detection of the α-form by WAXD was not consistent with scattering from individual nuclei, and the lack of any increase in the periodicity or invariant with time all but ruled out spinodal decomposition in the region probed. Individual nuclei involve too small a volume fraction to be detectable by SAXS or WAXD and too small to be seen by LS. As WAXD detects the crystallinity (>1%) in the sample, the gross morphology of the finite crystal lamellar stacks is already fully developed. These mechanisms are consistent with the recent rheo-optical study of the early stages of crystallization in iPP by Winter et al.,[42,43] who proposed that a gellike network is formed in the induction period.

We have shown that the WAXD α-form crystallinity is consistent with crystallinity on the basis of the predicted growth of the Avrami form and the measured intensity of the SAXS (lamellae) and LS (superstructure). Making trivial assumptions relating SAXS and LS to volume fraction of an ordered phase, the WAXD, SAXS, and LS data follow an expected Avrami form in the early stages of crystallization.

Acknowledgment. The authors gratefully acknowledge Dr. Fengji Yeh and Dr. Lizhi Liu (SUNYSB) for providing assistance during synchrotron measurements and Dr. Du-Fei Fang, Chris Kopp, Bruce X. Fu, and Haibo Hu for their help in light scattering studies. The authors are indebted to the helpful discussions with Professors Francisco Balta-Calleja, Stephen Z. D. Cheng, Benjamin Chu, Andrew Keller, Bernard Lotz, Richard S. Stein, and Jerold M. Schultz. The financial support of this work was provided by a grant from the NSF (DMR 9732653). The DOE grant (DE-FG02-99ER45760) for the support of the Advanced Polymers Beamline is also acknowledged.

Appendix

For characterizing the detection limit, solutions of *n*-tritriacontane ($C_{33}H_{68}$) in dodecane ($C_{12}H_{26}$) were prepared. The *n*-paraffin $C_{33}H_{68}$ (*n*-tritriacontane) was purchased from Aldrich Chemical Co., which had a purity of 98% and a melting temperature of 70.6 °C. The solvent dodecane ($C_{12}H_{26}$) was also purchased from Aldrich Chemical Co., which had a melting temperature of −9.7 °C. These samples were used as received. The solutions were first heated to 100 °C, where $C_{33}H_{68}$ and $C_{12}H_{26}$ were completely miscible. Then, the solutions were rapidly quenched to 0 °C in an ice bath, causing essentially complete precipitation of crystalline $C_{33}H_{68}$ in the form of a gellike structure. The X-ray measurements were carried out at 5 °C in a low-temperature chamber. Solutions of $C_{33}H_{68}$ in $C_{12}H_{26}$ with concentrations of 1.0, 4.1, and 7.8 wt % were prepared for this study. For the study of detection limit, simultaneous SAXS and WAXD measurements were performed on the solutions of $C_{33}H_{68}/C_{12}H_{26}$ at 5 °C with collection time of 300 s.

It is known that the detection limit of any analytical technique depends on the signal-to-noise ratio. As the sample concentration approaches zero, the signal disappears into the noise and the detection limit is reached. A quantitative definition of the detection limit thus can be defined as the concentration of sample that produces an output signal that is twice the root-mean-square of the background noise (a signal-to-noise ratio of 2, or S/N = 2).

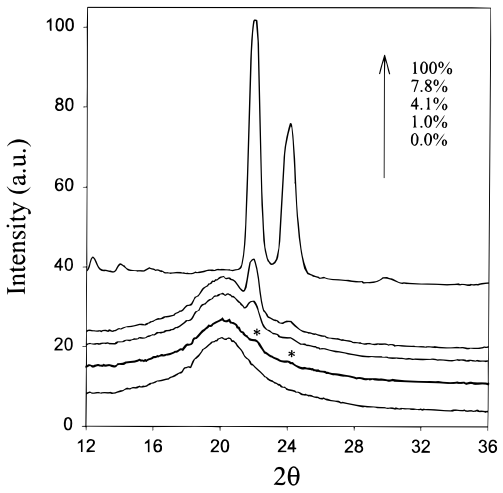

Figure 11. WAXD profiles of solutions of *n*-paraffin ($C_{33}H_{68}$) in dodecane ($C_{12}H_{26}$) at different concentrations measured at 5 °C.

When using simultaneous SAXS and WAXD techniques to follow the structural development during the early stages of crystallization, the most fundamental concern to be addressed is the difference between the detection limits of the different techniques. The detection limit for the SAXS technique documented in studies of dilute solutions is less than 0.3%.[22] Thus, the detection limit for SAXS may be assumed to be in the vicinity of 0.3%. However, this is not the case for WAXD. There is very little information available in the literature that may reveal the detection limit for WAXD. As we set to test the WAXD detection limit, one critical task is to develop means to prepare samples with controlled crystallinity at low values. This is difficult to accomplish by typical preparation schemes for polymers. In this study, we used a model system to prepare samples with known degrees of crystallinity. The prepared solutions showed viscous gellike properties, which consisted of *n*-tritriacontane ($C_{33}H_{68}$) with almost 100% crystallinity (similar to a pure polyethylene crystal) and dodecane (liquid) with no crystallinity (similar to the amorphous polyethylene melt). The lowest concentration (crystallinity) prepared in this study was 1%.

The WAXD profiles from the $C_{33}H_{68}/C_{12}H_{26}$ solutions at 5 °C are shown in Figure 11. In the SAXS profiles (not shown in this paper), no detectable signal (SAXS peaks) can be observed in the solutions. We attribute this to the large size of the $C_{33}H_{68}$ crystals (in microns), which falls beyond the detectable dimension of SAXS. By contrast, in crystals of pure $C_{33}H_{68}$, two scattering peaks at q values of 0.14 and 0.28 $Å^{-1}$ are clearly observed. These peaks represent the first- and second-order reflections from the lamellae corresponding to the length of the extended chain in the crystals.

In Figure 11, it is clear that WAXD detects crystal reflection peaks in all $C_{33}H_{68}/C_{12}H_{26}$ solutions including the one with a concentration (crystallinity) of 1.0% (marked with asterisk). The deconvolution analysis of the 1.0% WAXD profile is shown in Figure 12a. In this analysis, two Gaussian crystal reflection peaks (110) and (200) located at 22.2° and 24.2°and two Gaussian amorphous peaks at 20.5° were used to analyze the WAXD profile. The crystallinity (ϕ_{mc}) calculated from this deconvolution method was 0.94%, which was in good agreement with the designed crystallinity of 1.0%. Figure 12b shows the relationship between the measured and the designed crystallinity for all concentrations from the analysis of peak deconvolution. The slope 1.01 obtained from this plot indicated good agreement between the two values with an error margin of 1%. We have also evaluated the measured crystallinity using a different wavelength (1.54 Å) and obtained essentially the same result. This study verified that the WAXD technique has a detection limit as low as 1%.

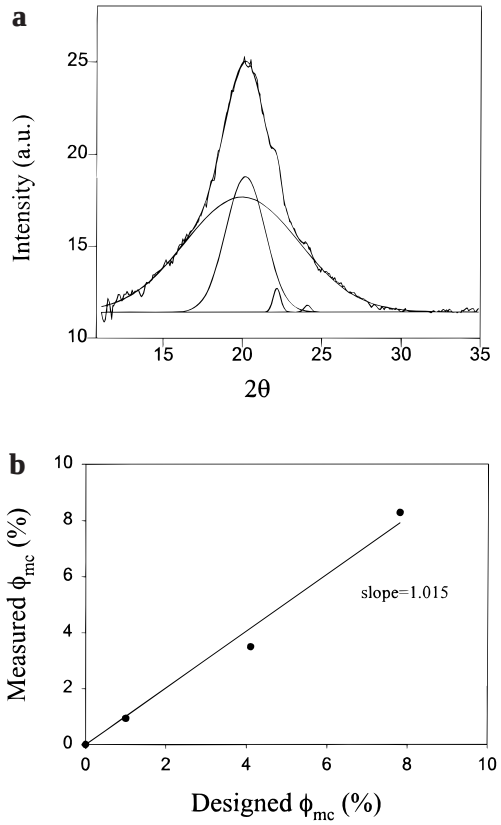

Figure 12. (a) Peak deconvolution analysis of a 1% *n*-paraffin ($C_{33}H_{68}$)/dodecane ($C_{12}H_{26}$) solution to separate the crystal reflections and amorphous background scattering. (b) Comparison of the measured and the designed crystallinity for solutions of *n*-paraffin ($C_{33}H_{68}$) in dodecane ($C_{12}H_{26}$).

In addition to the effect of concentration, there is another factor that can affect the detection of crystal reflection peaks by WAXD. This factor is the crystal size. It is known that if the crystal size is small, the reflection peaks can be broadened significantly according to the Scherrer equation:

$$L_{hkl} = \frac{k\lambda}{\beta_{hkl} \cos \theta} \qquad \text{(A1)}$$

where L_{hkl} is the crystallite size in the direction perpendicular to the reflection plane (hkl), K is the crystallite shape factor (0.89), λ is the wavelength, β_{hkl} is the reflection width at the half-maximum intensity, and θ is the Bragg angle of the particular reflection (2θ is the scattering angle). As the sizes of the $C_{33}H_{68}$ crystals were in the range of microns, it is necessary to evaluate the effect of crystal size of polymers on the WAXD detection at low crystallinity.

As it is experimentally difficult to prepare samples of low degrees of crystallinity with varying crystal sizes, we have used a modeling approach to tackle this problem. In this approach, the amorphous background was calculated using the two Gaussian functions ob-

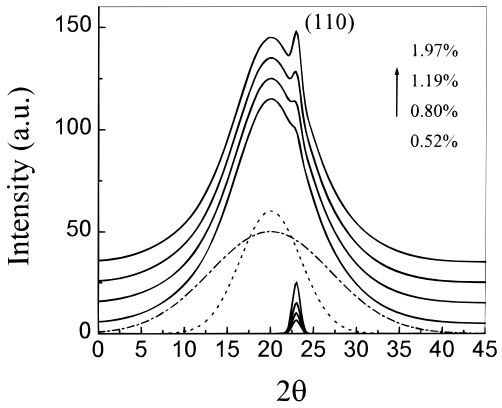

Figure 13. Simulated WAXD profiles for PE using the following parameters: $L_{110} = 20$ nm, $2\theta_{110} = 23°$, $X_{mc} = 0.52-1.97\%$

tained from Figure 12a, whereby only the strong (110) crystal reflection was used in the simulation. It was found that the crystallite size had a significant effect on the appearance of the crystal reflection. Figure 13 illustrates the calculated WAXD profiles using the crystal size (L_{110}) of 20 nm and varying (110) crystal fractions (X_{mc}, which is slightly smaller than the crystallinity ϕ_{mc} since the (200) reflection was not included here) (0.52−1.97%). The value of $L_{110} = 20$ nm seems to be a reasonable size to represent the smallest stable crystal dimension perpendicular to the (110) plane in PE, which is consistent with the estimates of the tips of the PE single crystals grown from solutions in TEM micrographs.[46] It is seen that detection of the (110) reflection becomes easier with an increase in crystal fraction. As the simulated crystal fraction is slightly larger than half of the programmed crystallinity (the fraction of the (110) peak is larger than that of the missing (200) peak), we conclude that the WAXD technique is capable of detecting crystallinity less than 1% with a minimum crystal size about 20 nm.

References and Notes

(1) Subirana, J. A. *Trends Polym. Sci.* **1997**, *5* (10), 321.
(2) Liu, C.; Muthukumar, M. *J. Chem. Phys.* **1998**, *109* (6), 1.
(3) Lee, C. H.; Saito, H.; Inoue, T.; Nojima, S. *Macromolecules* **1996**, *29*, 7034.
(4) Imai, M.; Mori, K.; Mizukami, T.; Kaji, K.; Kanaya, T. *Polymer* **1992**, *33*, 4451.
(5) Imai, M.; Kaji, K.; Kanaya, T.; Sakai, Y. *Phys. Rev. B* **1995**, *52*, 12696.
(6) Imai, M.; Mori, K.; Mizukami, T.; Kaji, K.; Kanaya, T. *Polymer* **1992**, *33*, 4457.
(7) Imai, M.; Kaji, K.; Kanaya, T. *Macromolecules* **1994**, *27*, 7103.
(8) Ezquerra, T. A.; López-Cabarcos, E.; Hsiao, B. S.; Baltà-Calleja, F. J. *Phys. Rev. E* **1996**, *54*, 989.
(9) Cahn, J. W.; Hilliard, J. E. *J. Chem. Phys.* **1958**, *28*, 258.
(10) Cahn, J. W. *J. Chem. Phys.* **1965**, *42*, 93.
(11) Ryan, A. J.; Terrill, N. J.; Fairclough, J. P. A. *ACS PMSE Prepr.* **1998**, *79*, 358.
(12) Terrill, N. J.; Fairclough, P. A.; Towns-Andrews, E.; Komanschek, B. U.; Young, R. J.; Ryan, A. J. *Polymer* **1998**, *39* (11), 2381.
(13) Olmsted, P. D.; Poon, W. C. K.; McLeish, T. C. B.; Terrill, N. J.; Ryan, A. J. *Phys. Rev. Lett.* **1998**, *81*, 373.
(14) Ostwald, W. *Z. Phys. Chem.* **1897**, *22*, 286.
(15) Hikosaka, M.; Rastogi, S.; Keller, A.; Kawabata, H. *J. Macromol. Sci.* **1992,** *B31*, 87.
(16) Rastogi, S.; Hikosaka, M.; Kawabata, H.; Keller, A. *Macromolecules* **1991,** *24*, 6384.
(17) Keller, A.; Hikosaka, M.; Rastogi, S. *Phys. Scr.* **1996**, *T66*, 243.
(18) Keller, A.; Hilosaka, M.; Rastogi, S.; Toda, A.; Barham, P. J.; Goldbeck-Wood, G. *J. Mater. Sci.* **1994**, *29*, 2579.
(19) Keller, A.; Cheng, S. Z. D. *Polymer* **1998**, *39*, 4461.
(20) Sirota, E. B.; Herhold, A. B. *Science* **1999**, *283*, 529.
(21) Sirota, E. B.; Herhold, A. B. In *Scattering from Polymers;* Cebe, P., Hsiao, B., Lohse, D., Eds.; ACS Symposium Book Series, in press.
(22) Glatter, O.; Kratky, O. *Small-Angle X-ray Scattering*; Academic Press: New York, 1982; Chapter 8, p 242.
(23) Lee, C. H.; Saito, H.; Inoue, T. *Macromolecules* **1993**, *26*, 6566.
(24) Okada, T.; Saito, H.; Inoue, T. *Macromolecules* **1992**, *25*, 1908.
(25) Cormia, R. L.; Price, F. P.; Turnbull, D. *J. Chem. Phys.* **1962**, *37*, 1333.
(26) Avrami, M. J. *J. Chem. Phys.* **1939**, *7*, 1103.
(27) Ross, G. S.; Frolen, L. J. *J. Res. Natl. Bur. Stand.* **1975**, *79A*, 701.
(28) Mandelkern, L.; Quinn, F. A.; Flory, P. J. *J. Appl. Phys.* **1954**, *25*, 830.
(29) Herhold, A.; Ertas, D.; Levine, A. J.; King, H. E. *Phys. Rev. E* **1999**, *59*, 6946.
(30) Hsiao, B. S.; Chu, B.; Yeh, F. NSLS July Newsletter, 1997, 1; http://bnlx27c.nsls.bnl.gov.
(31) Hsiao, B. S.; Gardner, K. H.; Wu, D. Q.; Chu, B. *Polymer* **1993**, *34* (19), 3996.
(32) Baltà-Calleja, F. J.; Vonk, G. G. *X-ray Scattering of Synthetic Polymers*; Elsevier Science: New York, 1989.
(33) Vonk, G. G. *Makromol. Chem. Macromol. Symp.* **1988**, *15*, 215.
(34) Hsiao, B. S.; Verma, R. K. *J. Synchrotron Radiat.* **1998**, *5*, 23.
(35) Strobl, G. R.; Schneider, M. *J. Polym. Sci., Polym. Phys. Ed.* **1980**, *18*, 1343.
(36) Stein, R. S.; Wilson, P. R. *J. Appl. Phys.* **1962**, *33*, 1914.
(37) Debye, P.; Bueche, A. M. *J. Appl. Phys.* **1949**, *20*, 518.
(38) Debye, P.; Anderson, H. R., Jr.; Brumberger, H. *J. Appl. Phys.* **1957**, *28*, 679.
(39) Verma, R. K.; Hsiao, B. S. *Trends Polym. Sci.* **1996**, *4* (10), 312.
(40) Verma, R. K.; Marand, H.; Hsiao, B. *Macromolecules* **1996**, *29*, 7767.
(41) Wang, Z. G.; Hsiao, B. S.; Sauer, B. B.; Kampert, W. G. *Polymer* **1999**, *40*, 4615.
(42) Pogodina, N. V.; Siddiquee, S. K.; van Egmond, J. W.; Winter, H. H. *Macromolecules* **1999,** *32* (4), 1167.
(43) Pogodina, N. V.; Winter, H. H. *Macromolecules* **1998**, *31*, 8164.
(44) Kim, C. Y.; Kim, Y. C.; Kim, S. C. *Polym. Sci. Eng.* **1993**, *33*, 1445.
(45) Natta, G.; Peraldo, M.; Corradini, P. *Rend. Accad. Naz. Lincei* **1959**, *26*, 14.
(46) Woodward, A. E. *Atlas of Polymer Morphology*; Hanser Publishers: Munich, 1996.

MA991468T